

---

# ProDAG: Projection-Induced Variational Inference for Directed Acyclic Graphs

---

**Ryan Thompson**  
University of Technology Sydney

**Edwin V. Bonilla**  
CSIRO's Data61

**Robert Kohn**  
University of New South Wales

## Abstract

Directed acyclic graph (DAG) learning is a rapidly expanding field of research. Though the field has witnessed remarkable advances over the past few years, it remains statistically and computationally challenging to learn a single (point estimate) DAG from data, let alone provide uncertainty quantification. Our article addresses the difficult task of quantifying graph uncertainty by developing a Bayesian variational inference framework based on novel distributions that have support directly on the space of DAGs. The distributions, which we use to form our prior and variational posterior, are induced by a projection operation, whereby an arbitrary continuous distribution is projected onto the space of sparse weighted acyclic adjacency matrices (matrix representations of DAGs) with probability mass on exact zeros. Though the projection constitutes a combinatorial optimization problem, it is solvable at scale via recently developed techniques that reformulate acyclicity as a continuous constraint. We empirically demonstrate that our method, **ProDAG**, can deliver accurate inference and often outperforms existing state-of-the-art alternatives.

dating back at least to the 1980s (Lauritzen and Spiegelhalter 1988; Pearl 1988), has recently witnessed a resurgence of interest due to a computational breakthrough by Zheng et al. (2018) that formulated a continuous characterization for the discrete notion of acyclicity. This breakthrough opened the door for scalable first-order algorithms that can learn DAG structures from datasets containing many more variables than previously considered feasible. We refer the reader to Vowels, Camgoz, and Bowden (2022) and Kitson et al. (2023) for recent surveys concerning this ongoing line of work.

Unlike maximum likelihood approaches that only learn point estimate DAGs (Zheng et al. 2018; Bello, Aragam, and Ravikumar 2022; Deng et al. 2023), Bayesian approaches learn entire posterior distributions over DAGs. The posterior quantifies graph uncertainty while acknowledging that the true DAG might be identifiable only up to its Markov equivalence class.<sup>1</sup> Uncertainty quantification also benefits downstream tasks such as treatment effect estimation (Geffner et al. 2022) and experimental design (Annadani et al. 2023b). Most Bayesian approaches use a Gibbs-type prior based on a continuous acyclicity penalty (Annadani et al. 2021; Lorch et al. 2021; Geffner et al. 2022) or model DAGs in an augmented space where acyclicity is readily satisfied (Charpentier, Kibler, and Günnemann 2022; Annadani et al. 2023a; Bonilla et al. 2024). While the former (Gibbs-type priors) do not guarantee an exact posterior over DAGs, the latter (augmented spaces) often require relaxations or inference over discrete structures.

Our article introduces **ProDAG**, a Bayesian method for learning DAGs that departs from the approaches above. Leveraging the benefits of variational inference, **ProDAG** models the prior and variational posterior using new distributions that directly have support on the space of DAGs. These DAG distributions are induced by mapping a continuous distribution  $\mathbb{P}$  onto the space of DAGs using a minimal distance projection. Consider a DAG represented by the weighted adjacency matrix  $W \in \mathbb{R}^{p \times p}$  with entries  $w_{jk}$  that are nonzero if and

## 1 INTRODUCTION

A directed acyclic graph (DAG) is graph with directed edges between nodes and no directed cycles, allowing it to represent complex conditional independencies compactly. DAGs play a central role in causal inference (Pearl 2009) and consequently have found applications spanning a broad range of domains such as psychology (Foster 2010), economics (Imbens 2020), and epidemiology (Tennant et al. 2021). The literature on DAGs,

---

Correspondence: Ryan Thompson  
Email: [ryan.thompson-1@uts.edu.au](mailto:ryan.thompson-1@uts.edu.au)

---

<sup>1</sup>The Markov equivalence class is the set of DAGs that encode the same conditional independencies.

only if there exists a directed edge from node  $j$  to node  $k$ . We induce a distribution over such matrices  $W$ , and hence over DAGs, using the data generating process

$$\tilde{W} \sim \mathbb{P}, \quad \lambda \sim \pi, \quad W = \text{proj}_\lambda(\tilde{W}), \quad (1)$$

where  $\lambda \geq 0$  is a parameter governing the graph’s sparsity (number of active edges) with prior  $\pi$  and

$$\text{proj}_\lambda(\tilde{W}) := \arg \min_{W \in \text{DAG}, \|W\|_{\ell_1} \leq \lambda} \frac{1}{2} \|\tilde{W} - W\|_F^2 \quad (2)$$

is the projection of  $\tilde{W} \in \mathbb{R}^{p \times p}$  onto the set of  $\ell_1$  constrained acyclic matrices.<sup>2</sup> We prove this projection is a measurable mapping with a unique solution, yielding valid probability distributions. One of the key qualities of these distributions is that they place probability mass on exact zeros, a necessity for sampling DAGs.

Inspired by recently developed continuous DAG characterizations (e.g., Zheng et al. 2018), we reformulate the combinatorial optimization problem (2) as an equivalent continuous optimization problem that can be solved in parallel on a GPU. We use this formulation in a variational framework by forming the prior and variational posterior using the new distributions, enabling scalable Bayesian DAG learning. Our framework accommodates DAGs represented as linear and nonlinear structural equation models (SEMs), making our approach suitable for problems and data of varying complexity. Experiments on synthetic and real data demonstrate that our approach often delivers more accurate inference than existing methods for DAG learning. Our toolkit implementing ProDAG is open-sourced.

## 2 RELATED WORK

Existing approaches for Bayesian inference on DAGs broadly fall into two categories: (1) regularization-based methods that include a continuous acyclicity penalty via a Gibbs-type prior in the variational objective (Annadani et al. 2021; Lorch et al. 2021; Geffner et al. 2022), and (2) state-augmentation methods that, e.g., place a prior over the graph’s topological ordering (Cundy, Grover, and Ermon 2021; Charpentier, Kibler, and Günnemann 2022; Bonilla et al. 2024). The node-potential augmentation of Annadani et al. (2023a) is related to the latter category. See also Wang, Wicker, and Kwiatkowska (2022) and Deleu et al. (2023) for approaches based on probabilistic circuits and generative flow networks. Our approach differs by designing a prior and approximate posterior directly over DAGs without modeling the topological ordering and without using a penalty that does not place mass on zeros.

<sup>2</sup>The norm  $\|W\|_{\ell_1} := \|\text{vec}(W)\|_1$ .

More broadly, our paper complements the literature on computational methods for point estimate DAG learning. The seminal paper of Zheng et al. (2018), which introduced the NOTEARS method, cleverly exploited the correspondence between the number of cycles in a matrix and the trace of that matrix’s power. A similar connection is now known to hold for other continuous functions and is exploited by methods such as DAGMA (Bello, Aragam, and Ravikumar 2022), which we utilize in this work, as well as those of Ng, Ghassami, and Zhang (2020), Yu et al. (2021), and Gillot and Parvainen (2022). These approaches that use continuous characterizations of acyclicity are appealing in that they scale to large graphs and can be augmented with discrete combinatorics (Manzour et al. 2021; Deng et al. 2023) if required. Though not pursued here, our DAG projection is also amenable to discrete techniques.

Finally, though distributions over DAGs via projection is a seemingly new idea, others have previously used projections to construct distributions over non-graphical structures. Xu and Duan (2023) designed distributions over sparse regression coefficients by projecting a vector drawn from an arbitrary continuous distribution onto the  $\ell_1$  ball. They illustrated several computational advantages of their distributions as priors in a Hamiltonian Monte Carlo (HMC) framework over classical spike-and-slab priors and prove that the resulting posterior enjoys the minimax concentration rate. Xu et al. (2023) extended this work to general proximal mappings with HMC, which includes the convex  $\ell_1$  projection as a special case. While our approach projects matrices onto the  $\ell_1$  ball, we also impose acyclicity, giving rise to a nonconvex combinatorial optimization problem that does not constitute a proximal mapping.

## 3 PROJECTION-INDUCED DISTRIBUTIONS

### 3.1 Description

To recap the introduction, we induce a distribution over weighted acyclic adjacency matrices  $W$  as  $W = \text{proj}_\lambda(\tilde{W})$ , where  $\text{proj}_\lambda$  is defined in (2),  $\tilde{W} \sim \mathbb{P}$  is a continuous matrix, and  $\lambda \sim \pi$  bounds the  $\ell_1$  norm of  $W$ . Since acyclic graphs have no self-loops (i.e.,  $W$  always has a zero diagonal), we can take  $\mathbb{P}$  to be any continuous distribution over the off-diagonal elements of  $\tilde{W}$  (e.g., a multivariate Gaussian), with the diagonal elements fixed as zero. The matrix  $\tilde{W}$  can thus be interpreted as the weighted adjacency matrix of a *simple directed graph*, with the projection removing all cycles.<sup>3</sup>

Besides removing cycles, the projection maps  $\tilde{W}$  onto

<sup>3</sup>Simple directed graphs have no self-loops and, at most, one edge in each direction between any pair of nodes.

an  $\ell_1$  ball of size  $\lambda$ . This part of the projection is necessary for sampling parsimonious graphs. Without this constraint, the projection would return the densest possible acyclic graph with  $(p^2 - p)/2$  edges.<sup>4</sup> The advantage of constraining  $W$  to an  $\ell_1$  ball, compared with modeling  $\tilde{W}$  as a Laplace distribution, is that it gives probability mass on exact zeros beyond that already given by the acyclicity constraint. It is known that Laplace distributions do not concentrate on zero except at their mode (Park and Casella 2008).

The resulting distribution  $p(W)$  can be understood as a mix of continuous components and exact zeros. To elaborate, first observe that the nonzeros in  $W$  may be indexed by a sparsity pattern  $S \in \{0, 1\}^{p \times p}$  (i.e., an unweighted acyclic adjacency matrix). The nonzeros are then given by  $W_S$ , where  $W_S$  is the restriction of  $W$  to  $S$ . Because the  $\ell_1$  constraint shrinks the nonzeros towards zero, the continuous  $W_S$  is a transformation  $f_\lambda$  of  $\tilde{W}_S$ , i.e.,  $W_S = f_\lambda(\tilde{W}_S)$ , where  $f_\lambda$  is implicitly given by the projection. This mixture interpretation suggests an interesting representation of  $p(W)$ :

$$\begin{aligned} p(W) &\equiv \sum_{i=1}^m p(W_{S_i} | S_i) p(S_i) \\ &= \sum_{i=1}^m p(f_\lambda(\tilde{W}_{S_i}) | S_i) p(S_i), \end{aligned}$$

where  $S_1, \dots, S_m$  is the finite collection of all acyclic adjacency matrices. To reiterate, the distributions  $p(f_\lambda(\tilde{W}_S) | S)$  and  $p(S)$  on the right-hand side are *implicitly* defined by the projection. Though this representation is conceptual, it highlights that  $p(W)$  forms a distribution over acyclic adjacency matrices  $S$  without explicitly having to model the discrete, high-dimensional probability mass function  $p(S)$ . Moreover, as we soon show, the projection can be reformulated as a continuous optimization problem, meaning it is unnecessary to deal with discreteness when sampling from  $p(W)$ .

### 3.2 Properties

One might ask if  $p(W)$  is a valid distribution. Theorem 1 addresses this question in the affirmative by showing that the projection is almost surely unique and measurable. The proof is in Appendix A.

**Theorem 1.** *Let  $\tilde{W}$  be endowed with a continuous probability measure. Then it holds:*

1. Projection (2) is unique almost surely with respect to the measure on  $\tilde{W}$ ; and
2. Projection (2) is measurable with respect to the measure on  $\tilde{W}$ .

<sup>4</sup>An exception is the degenerate case where some off-diagonal elements of  $\tilde{W}$  are already zero.

Theorem 1 states that, for continuous  $\tilde{W} \sim \mathbb{P}$ , the function  $\text{proj}_\lambda(\tilde{W})$  is uniquely defined and measurable. This result implies that a projection-induced distribution is a valid probability distribution since a measurable function  $g$  applied to a random variable  $z$  produces a well-defined random variable  $g(z)$ .

### 3.3 Graph Sparsity

To attain a distribution over graphs that contain a similar number of edges, the distribution  $\pi$  of  $\lambda$  can be specified as a Dirac delta distribution concentrated on a point  $\alpha \geq 0$  that yields the desired level of sparsity:

$$\pi_\alpha(\lambda) = \delta(\lambda - \alpha).$$

Alternatively, for graphs of varying complexity,  $\pi$  can be specified as a distribution over sparsity parameters  $\lambda \geq 0$ . For example,  $\pi$  can be taken as an exponential distribution parameterized by its mean  $\alpha \geq 0$ :

$$\pi_\alpha(\lambda) = \frac{\exp(-\lambda/\alpha)}{\alpha}, \quad \lambda \geq 0.$$

This specification allows for graphs with varying numbers of edges but favors sparser (parsimonious) graphs over denser graphs for smaller values of  $\alpha$ . The mean  $\alpha$  of  $\lambda$  can be determined using expert domain knowledge or empirically calibrated on an available validation set.

## 4 SCALABLE PROJECTIONS

### 4.1 Continuous Reformulation

To facilitate scalability, we reformulate the combinatorial projection (2) as an *equivalent* continuous optimization problem. This recharacterization follows recent work (Zheng et al. 2018; Bello, Aragam, and Ravikumar 2022) showing that for certain functions  $h(W)$  an important equivalence relationship holds:

$$h(W) = 0 \iff W \in \text{DAG}.$$

Bello, Aragam, and Ravikumar (2022) showed that for all matrices  $W \in \mathbb{W} := \{W \in \mathbb{R}^{p \times p} : \rho(W \circ W) < 1\}$ , where  $\rho$  is the spectral radius and  $\circ$  is the Hadamard product, the function  $h(W) := -\log \det(I - W \circ W)$  (DAGMA) has this property. This function attains the value zero if and only if there are no cycles in  $W$ , and thus, its level set at zero exactly corresponds to the set of DAGs. Though it is a nonconvex function, it is continuous and differentiable in  $W$ . We can thus rewrite projection (2) as the equivalent projection

$$\text{proj}_\lambda(\tilde{W}) = \arg \min_{W \in \mathbb{W}, h(W)=0, \|W\|_{\ell_1} \leq \lambda} \frac{1}{2} \|\tilde{W} - W\|_F^2. \quad (3)$$

As we discuss next, it is possible to solve this projection using only first-order methods for scalable posterior

learning and analytically evaluate the gradients of this projection for gradient-based posterior learning.

## 4.2 Algorithm

To solve projection (3), we use a two-step alternating procedure that produces a solution on the intersection of sets. Step 1 of this procedure projects  $\tilde{W}$  onto the set of acyclic matrices, yielding a matrix  $\hat{W}$ . Step 2 projects  $\hat{W}$  onto the  $\ell_1$  ball, yielding the final output  $W$  that remains acyclic but is further sparsified.

For the acyclicity projection, we use a path-following algorithm similar to Bello, Aragam, and Ravikumar (2022). This algorithm reformulates the problem by shifting the acyclicity constraint into the objective:

$$\min_{W \in \mathbb{W}} f_\mu(W; \tilde{W}) := \frac{\mu}{2} \|\tilde{W} - W\|_F^2 + h(W). \quad (4)$$

Here,  $\mu \geq 0$  is a coefficient taken along a sequence  $\mu^{(1)} > \mu^{(2)} > \dots > \mu^{(T)}$ . The path-following algorithm solves (4) at  $\mu = \mu^{(t+1)}$  by using the solution at  $\mu = \mu^{(t)}$  as an initialization point. The limiting solution as  $\mu \rightarrow 0$  is guaranteed to satisfy the acyclicity constraint  $h(W) = 0$  (Lemma 6, Bello, Aragam, and Ravikumar 2022). Algorithm 1 summarizes this procedure.

---

### Algorithm 1: Solver for acyclicity projection

---

**input** :  $\tilde{W} \in \mathbb{R}^{p \times p}$ ,  $\lambda \geq 0$ ,  $W^{(0)} \in \mathbb{W}$ ,  
 $\mu^{(1)} > \dots > \mu^{(T)} \geq 0$   
**for**  $t = 0, 1, \dots, T - 1$  **do**  
     Initialize  $W$  at  $W^{(t)}$  and set  
     
$$W^{(t+1)} \leftarrow \arg \min_{W \in \mathbb{W}} f_{\mu^{(t+1)}}(W; \tilde{W}) \quad (5)$$
  
**end**  
**output** :  $\hat{W} = W^{(T)}$

---

We take  $\mu^{(1)} = 1$ ,  $\mu^{(t+1)} = \mu^{(t)}/2$ ,  $T = 10$ , and  $W = 0 \in \mathbb{W}$ , which work well for our experiments. The inner optimization problem (5) is amenable to gradient descent. The gradient of  $f_\mu$  readily follows from the gradient of  $h$ , given by  $\nabla h(W) = 2(I - W \circ W)^{-1} \circ W$ .

For the  $\ell_1$  projection, we use an efficient (non-iterative) algorithm given by Duchi et al. (2008), which soft-thresholds the elements of the weighted adjacency matrix  $\hat{W}$  that is output by Algorithm 1. The soft-thresholding produces the final matrix  $W$ , which constitutes a solution to the original projection (3).

## 4.3 Gradients

In many Bayesian learning frameworks, including our variational framework, it is necessary to compute gradients. In our case, this computation is complicated by the presence of the projection since we need its gradients with respect to  $\tilde{W}$  and  $\lambda$ . Though it is technically

possible to differentiate through our algorithms using automatic differentiation (“autograd”), it is practically infeasible due to the iterative nature of Algorithm 1. As it turns out, it is possible to analytically evaluate the gradients via the implicit function theorem. This technique involves differentiating the Karush-Kuhn-Tucker (KKT) conditions of the projection that implicitly define  $W$  as a function of  $\tilde{W}$  and  $\lambda$ . The resulting gradients and their derivation are detailed in Appendix B.

## 5 POSTERIOR LEARNING

### 5.1 Variational Inference

Suppose we have data  $X \in \mathbb{R}^{n \times p}$ , containing  $n$  observations on  $p$  variables  $x \in \mathbb{R}^p$ . Let  $p(W)$  be a prior distribution over the weighted adjacency matrix  $W$ , taken here to be a projection-induced distribution. The conditional likelihood  $p(X | W)$  is given by the linear SEM  $x = W^\top x + \varepsilon$ , where  $\varepsilon \in \mathbb{R}^p$  is stochastic noise. Our task is to infer the posterior distribution  $p(W | X)$ . In general, this exact posterior is analytically intractable. Moreover, though our distribution admits a computationally convenient sampling algorithm, it is taxing to learn the posterior via traditional approaches (e.g., Markov chain Monte Carlo) due to it being high-dimensional. To this end, we use variational inference to approximate the posterior (see Blei, Kucukelbir, and McAuliffe 2017), leading to ProDAG.

Variational inference optimizes the parameters  $\theta$  of an approximate posterior  $q_\theta(W)$  such that it is nearest to the true posterior  $p(W | X)$  in Kullback-Leibler (KL) divergence. Like the prior, the approximate posterior is taken here to be a projection-induced distribution. However, as we discuss at the end of this section, performing variational inference on  $W$  alone is challenging because the projection is non-invertible. In other words, multiple unconstrained  $\tilde{W}$  can project to the same constrained (DAG)  $W$ . Towards this end, we focus on learning the joint posterior over  $W$  and  $\tilde{W}$ . The joint posterior does not suffer from non-invertibility because for any given  $W$ , the associated  $\tilde{W}$  is also observed.

Let  $p(\tilde{W}, W | X)$  be the true joint posterior and let  $q_\theta(\tilde{W}, W)$  be the variational joint posterior. Since  $W$  is a deterministic function of  $\tilde{W}$ , the variational joint posterior is the product of the variational marginal posterior  $q_\theta(\tilde{W})$  and a Dirac delta function:  $q_\theta(\tilde{W}, W) = q_\theta(\tilde{W})\delta(W - \text{proj}_\lambda(\tilde{W}))$ . The marginal  $q_\theta(\tilde{W})$  can be a continuous distribution, e.g., a multivariate Gaussian. The parameters  $\theta$  then contain means and covariances. Choosing  $q_\theta(\tilde{W})$  is the same as choosing  $\mathbb{P}$  in (1).



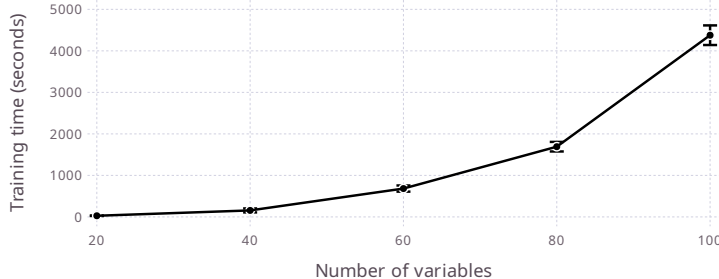


Figure 1: Training time in seconds as a function of the number of variables  $p$ . The averages (solid points) and standard errors (error bars) are measured over 10 independently and identically generated datasets.

## 5.2 Evidence Lower Bound

As in standard variational inference, we proceed by maximizing the evidence lower bound (ELBO):

$$\begin{aligned} \text{ELBO}(\theta) = \mathbb{E}_{q_\theta(\tilde{W}, W)}[\log p(X | \tilde{W}, W)] \\ - \text{KL}[q_\theta(\tilde{W}, W) \parallel p(\tilde{W}, W)]. \end{aligned} \quad (6)$$

The first term on the right-hand side of (6) is the expectation of the log-likelihood under the variational posterior. Since the log-likelihood depends only on  $\tilde{W}$  through  $W$ , this term is readily simplified as

$$\mathbb{E}_{q_\theta(\tilde{W}, W)}[\log p(X | \tilde{W}, W)] = \mathbb{E}_{q_\theta(W)}[\log p(X | W)].$$

To estimate this expectation, we sample DAGs from  $q_\theta(W)$  and evaluate the log-likelihood on these samples. To sample from  $q_\theta(W)$ , we need only sample from  $q_\theta(\tilde{W}, W)$  and discard  $\tilde{W}$ . The second term on the right-hand side of (6) is the KL divergence between the variational posterior  $q_\theta(\tilde{W}, W)$  and the prior  $p(\tilde{W}, W) = p(\tilde{W})\delta(W - \text{proj}_\lambda(\tilde{W}))$ . Since  $W$  is a deterministic function of  $\tilde{W}$ , the KL divergence between the joint posterior and prior is equal to the KL divergence between the marginal posterior and prior on  $\tilde{W}$ . Hence, the second term also can be simplified as

$$\text{KL}[q_\theta(\tilde{W}, W) \parallel p(\tilde{W}, W)] = \text{KL}[q_\theta(\tilde{W}) \parallel p(\tilde{W})].$$

Provided that  $q_\theta(\tilde{W})$  and  $p(\tilde{W})$  are chosen from distributional families with closed-form density functions (e.g., multivariate Gaussian distributions), this term is amenable to analytical evaluation. The gradients of Gaussians and other distributions for  $\tilde{W}$  are accommodated in the ELBO using the well-known reparameterization trick (see, e.g., Kingma and Welling 2014).

The challenge, mentioned earlier, of learning the marginal posterior of  $W$  alone arises due to the KL divergence appearing in (6). If we instead focus on the marginal posterior, the divergence term in (6) is between  $q_\theta(W)$  and  $p(W)$ . With some work, one can show that the divergence between these terms involves

the divergence between the (unknown) prior and posterior conditional distributions of  $\tilde{W}$  given  $W$ , since  $W$  is non-invertible in  $\tilde{W}$ . In any case, this issue is avoided altogether when learning the joint posterior.

## 5.3 Computational Complexity

As the preceding discussion indicates, the expected log-likelihood is the most computationally challenging component of the ELBO. Specifically, the forward pass during training projects a sample of  $\tilde{W}$  onto DAG space. This projection, performed by Algorithm 1, involves the inversion of  $p \times p$  matrices, an operation that has cubic complexity in the worst case. The backward pass is less expensive than the forward pass since the gradients of the projection (see Appendix B) only have quadratic complexity in  $p$ . Hence, the overall complexity of learning the variational posterior is  $O(p^3)$ .

Though cubic complexity is not ideal, many state-of-the-art frequentist and Bayesian approaches to DAG learning also exhibit cubic complexity (e.g., Lorch et al. 2021; Bello, Aragam, and Ravikumar 2022; Annadani et al. 2023a). Moreover, cubic complexity is the *worst case*. We investigate the *expected case* by plotting the average training time for a range of  $p$  in Figure 1. Though certainly not linear, the expected training time is seemingly much closer to quadratic than cubic.

# 6 NONLINEAR DAGS

## 6.1 Structural Equation Model

Our developments so far assume a linear SEM. However, our approach also accommodates nonlinear SEMs of the form  $x = f(x) + \varepsilon$ , where  $f : \mathbb{R}^p \rightarrow \mathbb{R}^p$  is a nonlinear function with an acyclic Jacobian matrix. Acyclicity of the Jacobian matrix is necessary because  $\partial f_k(x) / \partial x_j \neq 0$  indicates an edge exists from node  $j$  to node  $k$ . A standard choice of the function  $f$  is a neural network structured as  $f(x) = (f_1(x), \dots, f_p(x))^T$ , where  $f_k(x)$  is a feedforward sub-network that models node  $k$ .

Let  $\omega = (\omega_1, \dots, \omega_p)$  be a  $p$ -tuple of neural network weights corresponding to  $f_1, \dots, f_p$ . Denote by  $\omega_k^h \in \mathbb{R}^{p \times d}$  the restriction of the  $k$ th network’s weights  $\omega_k$  to the first hidden layer, where  $d$  is the number of neurons in that layer. If the  $j$ th row of  $\omega_k^h$ , denoted  $\omega_{jk}^h \in \mathbb{R}^d$ , is a zero vector (i.e.,  $\|\omega_{jk}^h\|_2 = 0$ ), then  $\partial f_k(x)/\partial x_j = 0$  and no edge exists from node  $j$  to node  $k$ . Hence, we can enforce acyclicity on the Jacobian of  $f(x)$  by enforcing acyclicity on the  $p \times p$  matrix  $W(\omega) := [\|\omega_{jk}^h\|_2]$ .

## 6.2 Prior and Posterior

In the nonlinear SEM setting, we induce a DAG distribution over *all* weights  $\omega$  of the neural network as

$$\tilde{\omega} \sim \mathbb{P}, \quad \lambda \sim \pi, \quad \omega = \text{proj}_\lambda(\tilde{\omega}),$$

where  $\mathbb{P}$  is a continuous distribution over the weights. This data generating process yields a *fully Bayesian* neural network with every layer having a prior over its weights. The projection here modifies our earlier projection to now seek the weights  $\omega$  nearest to  $\tilde{\omega}$  such that the adjacency matrix  $W(\omega)$  is acyclic and sparse:

$$\text{proj}_\lambda(\tilde{\omega}) := \arg \min_{\substack{W(\omega) \in \mathbb{W}, h(W(\omega))=0 \\ \|W(\omega)\|_{\ell_1} \leq \lambda}} \frac{1}{2} \sum_{k=1}^p \|\tilde{\omega}_k - \omega_k\|_F^2. \quad (7)$$

The matrix  $W(\omega)$  that characterizes the constraints in (7) is a function only of the *first* hidden layer weights. Hence, the projection only modifies those weights and leaves the weights of the remaining layers untouched.

Though the weights on the input layer are significantly more numerous than in the linear case (specifically  $d$  times as many weights), the projection is able to be reduced to a simpler problem that is no more computationally taxing than the linear case. Proposition 1 presents this result. The proof is in Appendix C.

**Proposition 1.** *Let  $\tilde{\omega}$  be a tuple of neural network weights and let  $\tilde{\omega}_{jk}^h$  be the vector of weights for the  $j$ th input to the first hidden layer of the  $k$ th output. Define the matrix  $\tilde{W}$  elementwise as  $\tilde{w}_{jk} = \|\tilde{\omega}_{jk}^h\|_2$  and let  $W$  be the projection of  $\tilde{W}$  in (3). Then projection (7) is solved by taking  $\omega_{jk}^h = \tilde{\omega}_{jk}^h \mathbf{w}_{jk} / \tilde{w}_{jk}$  for  $j, k = 1, \dots, p$  and leaving the remaining layers’ weights unmodified.*

Proposition 1 states that we need only project the matrix  $\tilde{W}$  constructed from  $\tilde{\omega}$  to obtain the weights  $\omega$  for an acyclic neural network  $f(x)$ . Consequently, the nonlinear SEM setting requires no new algorithms.

Performing posterior inference for the neural network weights  $\omega$  within our variational framework also requires no major modifications. The only change required is to re-express the ELBO in terms of  $\omega$ , yielding

$$\text{ELBO}(\theta) = \mathbb{E}_{q_\theta(\omega)}[\log p(X | \omega)] - \text{KL}[q_\theta(\tilde{\omega}) \parallel p(\tilde{\omega})],$$

where the variational parameters  $\theta$  now parameterize a distribution whose dimensionality is the same as  $\omega$ .

## 7 EXPERIMENTS

### 7.1 Toolkit

To enable experiments on data, we implement ProDAG in a Julia (Bezanson et al. 2017) toolkit, built using the machine learning library Flux (Innes et al. 2018). Our toolkit handles linear and nonlinear DAGs and rapidly performs projections using parallel (batched CUDA) implementations of the projection algorithms. It is publicly available as an open-source package at

<https://github.com/ryan-thompson/ProDAG.jl>.

### 7.2 Baselines and Metrics

Our method ProDAG is benchmarked against several state-of-the-art methods: DAGMA (Bello, Aragam, and Ravikumar 2022), DiBS and DiBS+ (Lorch et al. 2021), and BayesDAG (Annadani et al. 2023a). DAGMA is a frequentist version of our approach that delivers a point estimate DAG. DiBS, DiBS+, and BayesDAG are Bayesian approaches that learn posterior distributions over DAGs. Appendix D describes each method’s hyperparameters and implementation. In addition to these state-of-the-art methods, we include PC (Spirtes, Glymour, and Scheines 2001) as a classic baseline.

We consider several metrics that characterize different qualities of the learned posterior distributions. As a measure of uncertainty quantification, we report the Brier score under the posterior. As measures of structure recovery, we report the expected structural Hamming distance (SHD) and expected F1 score under the posterior. Finally, as a measure of discriminative power, we report the AUROC under the posterior. Lower values of Brier score and expected SHD are better, while higher values of expected F1 score and AUROC are better. All four metrics compare the learned posterior to the ground truth DAG. Since DAGMA and PC return a single point estimate graph, the metrics are evaluated by taking its posterior as a Dirac delta distribution that places all mass on the learned graph. For ProDAG, DiBS, DiBS+, and BayesDAG, the metrics are evaluated on a sample of graphs drawn from the learned posterior.

### 7.3 Linear Synthetic Data

Figures 2 and 3 report results on datasets simulated from linear DAGs with  $p = 20$  and  $p = 100$  variables, respectively. The sample size is varied between  $n = 10$  and  $n = 1000$ . Appendix E describes the full design.

ProDAG delivers comparatively strong performance

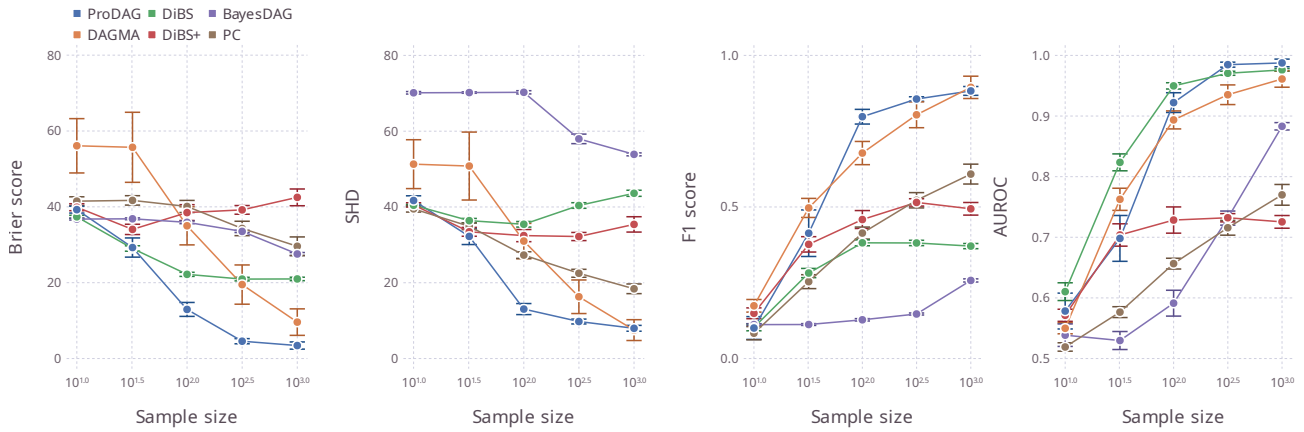


Figure 2: Performance on *linear* synthetic data with  $p = 20$  variables and 40 edges. The averages (solid points) and standard errors (error bars) are measured over 10 independently and identically generated datasets.

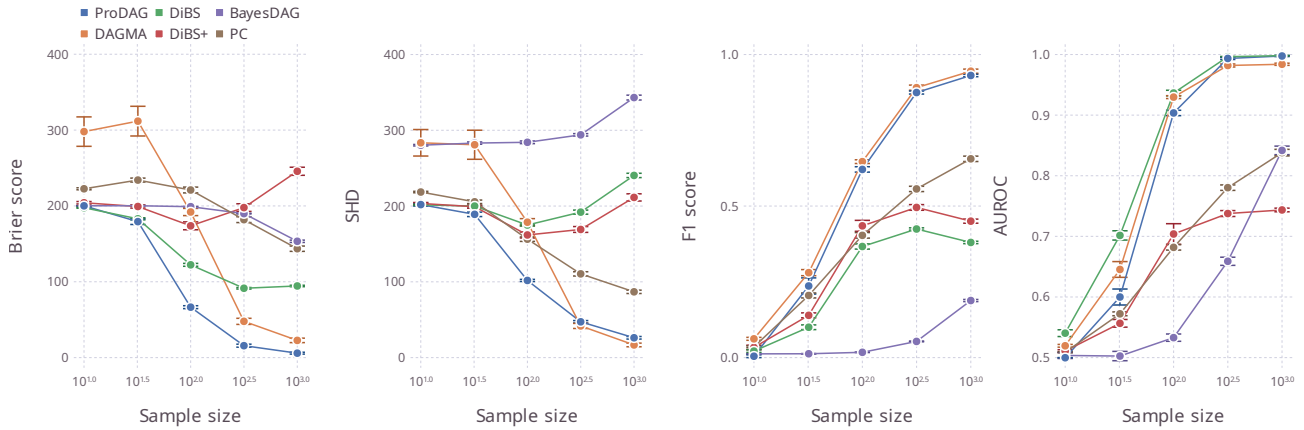


Figure 3: Performance on *linear* synthetic data with  $p = 100$  variables and 200 edges. The averages (solid points) and standard errors (error bars) are measured over 10 independently and identically generated datasets.

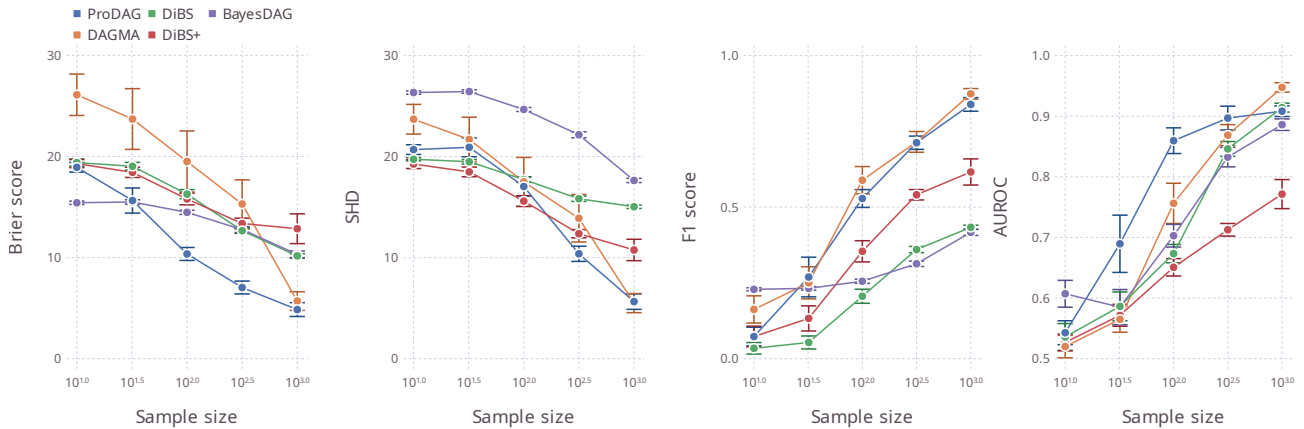


Figure 4: Performance on *nonlinear* synthetic data with  $p = 10$  variables and 20 edges. The averages (solid points) and standard errors (error bars) are measured over 10 independently and identically generated datasets.

Table 1: Performance on the flow cytometry dataset of Sachs et al. (2005). The dataset consists of  $n = 7466$  observations,  $p = 11$  variables, and 18 edges. The best achieved value of each metric is indicated in boldface.

	Brier score	Expected SHD	Expected F1 score	AUROC
ProDAG	19.3	<b>20.9</b>	<b>0.33</b>	<b>0.66</b>
DAGMA	27.0	24.0	0.27	0.57
DiBS	<b>18.5</b>	26.2	0.15	0.55
DiBS+	32.0	30.0	0.06	0.45
BayesDAG	20.4	26.0	0.23	0.59

across the full suite of sample sizes, especially regarding uncertainty quantification. For small sample sizes, where there is little hope of recovering the true graph, ProDAG is as competitive as other Bayesian methods. Meanwhile, for moderate and large sample sizes, ProDAG overtakes the Bayesian methods across most metrics. ProDAG even performs as well as the frequentist DAGMA for the largest sample size, where little uncertainty remains regarding the true graph. Except for their discriminative power, measured by AUROC, DiBS and BayesDAG do not significantly improve with the sample size. Lorch et al. (2021) studied DiBS on a sample size of  $n = 100$ , and their results roughly match ours at  $n = 100$ . Annadani et al. (2023a) evaluated BayesDAG on much smaller graphs of size  $p = 5$ .

#### 7.4 Nonlinear Synthetic Data

Figure 4 reports results on datasets simulated from nonlinear DAGs. Following Zheng et al. (2020), each variable in the graph is generated from a single hidden-layer neural network whose inputs are that variable’s parents. The learning task is more challenging here than in the linear setting (approximately  $10\times$  more unknown parameters for a graph of the same size), so the number of variables is fixed to  $p = 10$ . PC handles linear DAGs only, so it is excluded as a baseline here.

For the most part, the story here is similar to the linear setting: ProDAG delivers strong performance and improves over the frequentist and Bayesian baselines most of the time. Again, it particularly excels at uncertainty quantification. The results for DiBS approximately match those in Lorch et al. (2021), where its expected SHD is similar to that of the null graph. Annadani et al. (2023a) studied BayesDAG on a sample size of  $n = 5000$ , much bigger than the largest sample size here. ProDAG does not appear to require a sample of similarly large size to produce high-quality inference.

#### 7.5 Real Data

The flow cytometry data of Sachs et al. (2005) is a biological dataset designed to aid the discovery of protein

signaling networks. The dataset contains  $n = 7466$  human cell measurements on  $p = 11$  phosphoproteins and phospholipids. Notably, it is one of the few real datasets with an expert consensus graph available. For this reason, it has become a widely adopted dataset for real-world evaluation of DAG learning approaches.

Table 1 reports results on the flow cytometry dataset, with the consensus graph (consisting of 18 directed edges) taken as the ground truth. To accommodate possible nonlinearities, each approach learns a posterior over nonlinear DAGs. ProDAG outperforms all approaches in expected SHD, expected F1 score, and AUROC while only just underperforming DiBS in terms of Brier score. Even so, the F1 score from ProDAG is more than twice that of DiBS. Meanwhile, ProDAG uniformly improves on DAGMA. This result highlights the Bayesian benefits of ProDAG over DAGMA, since both approaches are otherwise identical in their characterization of acyclicity via the log determinant function.

## 8 CONCLUDING REMARKS

DAGs are inherently complex structures due to their acyclic nature, making Bayesian inference a formidable task, both statistically and computationally. This paper introduces ProDAG, a novel approach to the problem that employs new projection-induced distributions that have support directly on the space of DAGs. We study some key properties of these distributions and show they indeed constitute valid probability distributions. Moreover, we demonstrate that they lead to accurate inference when used as a prior and approximate posterior in a variational framework. As an important extension, our approach generalizes to accommodate nonlinear DAGs formulated as acyclic neural networks, widening its applicability to diverse problems and data.

## References

Annadani, Y., Pawlowski, N., Jennings, J., Bauer, S., Zhang, C., and Gong, W. (2023a). “BayesDAG: Gradient-based posterior inference for causal discov-



- ery”. *Advances in Neural Information Processing Systems*. Vol. 36, pp. 1738–1763.
- Annadani, Y., Rothfuss, J., Lacoste, A., Scherrer, N., Goyal, A., Bengio, Y., and Bauer, S. (2021). “Variational causal networks: Approximate Bayesian inference over causal structures”. arXiv: 2106.07635.
- Annadani, Y., Tigas, P., Ivanova, D. R., Jesson, A., Gal, Y., Foster, A., and Bauer, S. (2023b). “Differentiable multi-target causal Bayesian experimental design”. *Proceedings of the 40th International Conference on Machine Learning*. Vol. 202, pp. 34263–34279.
- Bello, K., Aragam, B., and Ravikumar, P. (2022). “DAGMA: Learning DAGs via M-matrices and a log-determinant acyclicity characterization”. *Advances in Neural Information Processing Systems*. Vol. 35, pp. 8226–8239.
- Bezanson, J., Edelman, A., Karpinski, S., and Shah, V. B. (2017). “Julia: A fresh approach to numerical computing”. *SIAM Review* 59 (1), pp. 65–98.
- Blei, D. M., Kucukelbir, A., and McAuliffe, J. D. (2017). “Variational inference: A review for statisticians”. *Journal of the American Statistical Association* 112 (518), pp. 859–877.
- Bonilla, E. V., Elinas, P., Zhao, H., Filippone, M., Kitsios, V., and O’Kane, T. (2024). “Variational DAG estimation via state augmentation with stochastic permutations”. arXiv: 2402.02644.
- Charpentier, B., Kibler, S., and Günnemann, S. (2022). “Differentiable DAG sampling”. *International Conference on Learning Representations*.
- Cundy, C., Grover, A., and Ermon, S. (2021). “BCD Nets: Scalable variational approaches for Bayesian causal discovery”. *Advances in Neural Information Processing Systems*. Vol. 34, pp. 7095–7110.
- Deleu, T., Nishikawa-Toomey, M., Subramanian, J., Malkin, N., Charlin, L., and Bengio, Y. (2023). “Joint Bayesian inference of graphical structure and parameters with a single generative flow network”. *Advances in Neural Information Processing Systems*. Vol. 36, pp. 31204–31231.
- Deng, C., Bello, K., Aragam, B., and Ravikumar, P. (2023). “Optimizing NOTEARS objectives via topological swaps”. *Proceedings of the 40th International Conference on Machine Learning*. Vol. 202, pp. 7563–7595.
- Duchi, J., Shalev-Shwartz, S., Singer, Y., and Chandra, T. (2008). “Efficient projections onto the  $\ell_1$ -ball for learning in high dimensions”. *Proceedings of the 25th International Conference on Machine Learning*, pp. 272–279.
- Foster, E. M. (2010). “Causal inference and developmental psychology”. *Developmental Psychology* 46 (6), pp. 1454–1480.
- Geffner, T., Antoran, J., Foster, A., Gong, W., Ma, C., Kiciman, E., Sharma, A., Lamb, A., Kukla, M., Hilmkil, A., Jennings, J., Pawlowski, N., Allamanis, M., and Zhang, C. (2022). “Deep end-to-end causal inference”. *NeurIPS 2022 Workshop on Causal Machine Learning for Real-World Impact*.
- Gillot, P. and Parviainen, P. (2022). “Learning large DAGs by combining continuous optimization and feedback arc set heuristics”. *Proceedings of the AAAI Conference on Artificial Intelligence*. Vol. 36, pp. 6713–6720.
- Imbens, G. W. (2020). “Potential outcome and directed acyclic graph approaches to causality: Relevance for empirical practice in economics”. *Journal of Economic Literature* 58 (4), pp. 1129–1179.
- Innes, M. J., Saba, E., Fischer, K., Gandhi, D., Rudilosso, M. C., Joy, N. M., Karmali, T., Pal, A., and Shah, V. B. (2018). “Fashionable modelling with Flux”. *Workshop on Systems for ML and Open Source Software at NeurIPS 2018*.
- Kingma, D. P. and Ba, J. L. (2015). “Adam: A method for stochastic optimization”. *International Conference on Learning Representations*.
- Kingma, D. P. and Welling, M. (2014). “Auto-encoding variational Bayes”. *International Conference on Learning Representations*.
- Kitson, N. K., Constantinou, A. C., Guo, Z., Liu, Y., and Chobtham, K. (2023). “A survey of Bayesian network structure learning”. *Artificial Intelligence Review* 56 (8), pp. 8721–8814.
- Lauritzen, S. L. and Spiegelhalter, D. J. (1988). “Local computations with probabilities on graphical structures and their application to expert systems”. *Journal of the Royal Statistical Society: Series B (Methodological)* 50 (2), pp. 157–224.
- Lorch, L., Rothfuss, J., Schölkopf, B., and Krause, A. (2021). “DiBS: Differentiable Bayesian structure learning”. *Advances in Neural Information Processing Systems*. Vol. 34, pp. 24111–24123.
- Manzour, H., Küçükyavuz, S., Wu, H.-H., and Shojaie, A. (2021). “Integer programming for learning directed acyclic graphs from continuous data”. *INFORMS Journal on Optimization* 3 (1), pp. 46–73.
- Ng, I., Ghassami, A., and Zhang, K. (2020). “On the role of sparsity and DAG constraints for learning linear DAGs”. *Advances in Neural Information Processing Systems*. Vol. 33, pp. 17943–17954.
- Park, T. and Casella, G. (2008). “The Bayesian lasso”. *Journal of the American Statistical Association* 103 (482), pp. 681–686.
- Pearl, J. (1988). *Probabilistic Reasoning in Intelligent Systems. Networks of Plausible Inference*. San Francisco, USA: Morgan Kaufmann.
- (2009). *Causality: Models, Reasoning, and Inference*. 2nd. New York, USA: Cambridge University Press.
- Sachs, K., Perez, O., Pe’er, D., Lauffenburger, D. A., and Nolan, G. P. (2005). “Causal protein-signaling

- networks derived from multiparameter single-cell data”. *Science* 308 (5721), pp. 523–529.
- Spirites, P., Glymour, C., and Scheines, R. (2001). *Causation, Prediction, and Search*. MIT Press.
- Tennant, P. W. G., Murray, E. J., Arnold, K. F., Berrie, L., Fox, M. P., Gadd, S. C., Harrison, W. J., Keeble, C., Ranker, L. R., Textor, J., Tomova, G. D., Gilthorpe, M. S., and Ellison, G. T. H. (2021). “Use of directed acyclic graphs (DAGs) to identify confounders in applied health research: Review and recommendations”. *International Journal of Epidemiology* 50 (2), pp. 620–632.
- Thompson, R., Bonilla, E. V., and Kohn, R. (2024). “Contextual directed acyclic graphs”. *Proceedings of the 27th International Conference on Artificial Intelligence and Statistics*. Vol. 238, pp. 2872–2880.
- Vowels, M. J., Camgoz, N. C., and Bowden, R. (2022). “D’ya like DAGs? A survey on structure learning and causal discovery”. *ACM Computing Surveys* 55 (4), pp. 1–36.
- Wang, B., Wicker, M., and Kwiatkowska, M. (2022). “Tractable uncertainty for structure learning”. *Proceedings of the 39th International Conference on Machine Learning*. Vol. 162, pp. 23131–23150.
- Xu, M. and Duan, L. L. (2023). “Bayesian inference with the  $l_1$ -ball prior: Solving combinatorial problems with exact zeros”. *Journal of the Royal Statistical Society: Series B (Statistical Methodology)* 85 (5), pp. 1538–1560.
- Xu, M., Zhou, H., Hu, Y., and Duan, L. L. (2023). “Bayesian inference using the proximal mapping: Uncertainty quantification under varying dimensionality”. *Journal of the American Statistical Association*.
- Yu, Y., Gao, T., Yin, N., and Ji, Q. (2021). “DAGs with no curl: An efficient DAG structure learning approach”. *Proceedings of the 38th International Conference on Machine Learning*. Vol. 139, pp. 12156–12166.
- Yuan, M. and Lin, Y. (2006). “Model selection and estimation in regression with grouped variables”. *Journal of the Royal Statistical Society: Series B (Statistical Methodology)* 68 (1), pp. 49–67.
- Zheng, X., Aragam, B., Ravikumar, P., and Xing, E. P. (2018). “DAGs with NO TEARS: Continuous optimization for structure learning”. *Advances in Neural Information Processing Systems*. Vol. 31.
- Zheng, X., Dan, C., Aragam, B., Ravikumar, P., and Xing, E. P. (2020). “Learning sparse nonparametric DAGs”. *Proceedings of the 23rd International Conference on Artificial Intelligence and Statistics*. Vol. 108, pp. 3414–3425.

## A PROOF OF THEOREM 1

*Proof.* We proceed by proving the each claim of the theorem in turn.

**Uniqueness** We begin by proving the first claim that the projection is unique almost surely. First, observe that the weighted adjacency matrix  $W$  can be expressed in terms of an adjacency matrix  $S$  and a continuous matrix  $V$ :

$$\min_{W \in \text{DAG}, \|W\|_{\ell_1} \leq \lambda} \|\tilde{W} - W\|_F^2 \iff \min_{\substack{S \in \{0,1\}^{p \times p}, S \in \text{DAG} \\ V \in \mathbb{R}^{p \times p}, \|V\|_{\ell_1} \leq \lambda}} f_S(V; \tilde{W}) := \|\tilde{W} - S \odot V\|_F^2,$$

where  $\odot$  denotes the Hadamard product and we adopt the convention that  $v_{jk} = 0$  if  $s_{jk} = 0$ . We can write the minimization on the right-hand side as a min-min problem:

$$\min_{\substack{S \in \{0,1\}^{p \times p}, S \in \text{DAG} \\ V \in \mathbb{R}^{p \times p}, \|V\|_{\ell_1} \leq \lambda}} f_S(V; \tilde{W}) \iff \min_{S \in \{0,1\}^{p \times p}, S \in \text{DAG}} \min_{V \in \mathbb{R}^{p \times p}, \|V\|_{\ell_1} \leq \lambda} f_S(V; \tilde{W}).$$

Consider the inner optimization problem on the right-hand side. Let  $V^*$  denote an optimal solution to this problem, and define the set of non-unique solutions as

$$A_S := \{\tilde{W} \in \mathbb{R}^{p \times p} \mid f_S(V_1^*; \tilde{W}) = f_S(V_2^*; \tilde{W}), V_1^* \neq V_2^*\}.$$

Since  $f_S(V; \tilde{W})$  is strictly convex in  $V$  and continuous and  $\tilde{W}$ , the optimal objective value  $f_S(V^*; \tilde{W})$  is continuous and unique with respect to the measure on  $\tilde{W}$ . Hence, the set  $A_S$  has measure zero with respect to  $\tilde{W}$ . Now, define the set of non-unique solutions across any two different adjacency matrices  $S_1$  and  $S_2$  as

$$A_{S_1, S_2} := \{\tilde{W} \in \mathbb{R}^{p \times p} \mid f_{S_1}(V_1^*; \tilde{W}) = f_{S_2}(V_2^*; \tilde{W}), V_1^* \neq V_2^*\}.$$

Since  $S_1$  and  $S_2$  simply induce different subspaces over  $\tilde{W}$ , the set  $A_{S_1, S_2}$  also has measure zero. Moreover, the union of  $A_{S_1, S_2}$  over all adjacency matrices  $S_1 \neq S_2$  has measure zero. We conclude that the projection is unique almost surely.

**Measurability** To prove the second claim that the projection is measurable, define the functions

$$g_\lambda(\tilde{W}, S) := \arg \min_{\substack{V \in \mathbb{R}^{p \times p} \\ \|V\|_{\ell_1} \leq \lambda}} \|\tilde{W} - S \odot V\|_F^2,$$

and

$$h_\lambda(\tilde{W}) := \arg \min_{\substack{S \in \{0,1\}^{p \times p} \\ S \in \text{DAG}}} \|\tilde{W} - S \odot g_\lambda(\tilde{W}, S)\|_F^2.$$

It follows that

$$\text{proj}_\lambda(\tilde{W}) = g_\lambda(\tilde{W}, h_\lambda(\tilde{W})).$$

We now demonstrate that each of these functions are measurable in  $\tilde{W}$ . First, for fixed  $S$ , the function  $g_\lambda(\tilde{W}, S)$  is the minimizing argument of a convex optimization problem and hence continuous in  $\tilde{W}$ . Continuous functions are measurable with respect to their argument, and therefore  $g_\lambda(\tilde{W}, S)$  is measurable in  $\tilde{W}$ . Second, since the set of acyclic adjacency matrices is finite, the function  $h_\lambda(\tilde{W})$  takes the pointwise minimum of finitely many measurable functions and returns the adjacency matrix indexed by that minimum. A pointwise minimum of measurable functions is itself measurable. Lastly, since  $g_\lambda(\tilde{W}, S)$  and  $h_\lambda(\tilde{W})$  are both measurable in  $\tilde{W}$ , their composition  $g_\lambda(\tilde{W}, h_\lambda(\tilde{W}))$  must also be measurable in  $\tilde{W}$ . We conclude that  $\text{proj}_\lambda(\tilde{W})$  is measurable in  $\tilde{W}$ .  $\square$

## B GRADIENTS

Proposition 2 presents the gradients of the minimizer in (3) with respect to the continuous matrix  $\tilde{W}$  and the sparsity parameter  $\lambda$ . The proof is at the end of this section.

**Proposition 2.** Let  $W = (w_{jk}) \in \mathbb{R}^{p \times p}$  be the output of projection (3) applied to the matrix  $\tilde{W} = (\tilde{w}_{jk}) \in \mathbb{R}^{p \times p}$  with sparsity parameter  $\lambda > 0$ . Let  $\mathcal{A} := \{(j, k) : w_{jk} \neq 0\}$  be the set of active edge weights. Then, if the  $\ell_1$  constraint is binding, the gradients of  $w_{jk}$  with respect to  $\tilde{w}_{jk}$  and  $\lambda$  are

$$\frac{\partial w_{jk}}{\partial \tilde{w}_{qr}} = \begin{cases} \delta_{jk}^{qr} - \frac{\text{sign}(w_{qr}) \text{sign}(w_{jk})}{|\mathcal{A}|} & \text{if } (j, k) \in \mathcal{A} \\ 0 & \text{otherwise} \end{cases} \quad \text{and} \quad \frac{\partial w_{jk}}{\partial \lambda} = \begin{cases} \frac{\text{sign}(w_{jk})}{|\mathcal{A}|} & \text{if } (j, k) \in \mathcal{A} \\ 0 & \text{otherwise,} \end{cases}$$

where  $\delta_{jk}^{qr} := 1[(j, k) = (q, r)]$  and  $|\mathcal{A}|$  is the cardinality of  $\mathcal{A}$ . Otherwise, if the  $\ell_1$  constraint is non-binding, the gradients are

$$\frac{\partial w_{jk}}{\partial \tilde{w}_{qr}} = \begin{cases} \delta_{jk}^{qr} & \text{if } (j, k) \in \mathcal{A} \\ 0 & \text{otherwise} \end{cases} \quad \text{and} \quad \frac{\partial w_{jk}}{\partial \lambda} = 0.$$

Proposition 2 indicates that the Jacobian is sparse and has nonzeros only in positions corresponding to the surviving elements in  $W$ . In the binding case, where the  $\ell_1$  constraint has a shrinkage effect, the value of the nonzeros depends on the size of the active set  $\mathcal{A}$  (the number of nonzero edges). In the non-binding case, where the  $\ell_1$  constraint imparts no shrinkage, all nonzero components equal one. Importantly, Proposition 2 indicates that only the projection's output  $W$  is needed to evaluate the gradients; no additional computations are required. This result is useful for posterior learning since it means that a backward pass through the model demands virtually no further overhead cost.

Thompson, Bonilla, and Kohn (2024) presented a result related to Proposition 2 in which they provided the gradients of a DAG projection for contextual learning. Their gradients differ slightly from those here because their sparsity constraint is different. The gradients relating to  $\lambda$  were not considered in their work. Our proof strategy roughly follows theirs.

*Proof.* Let  $W^*$  denote an optimal solution to projection (3). The KKT conditions for stationarity and complementary slackness are

$$\partial \left( \frac{1}{2} \|\tilde{W} - W^*\|_F^2 + \nu^* (\|W^*\|_{\ell_1} - \lambda) + \eta^* h(W^*) \right) \ni 0 \quad (8)$$

and

$$\nu^* (\|W^*\|_{\ell_1} - \lambda) = 0, \quad (9)$$

where  $\nu^*$  and  $\eta^*$  are the optimal values of the KKT multipliers. The optimal solution  $W^*$  is implicitly a function of the problem data  $\tilde{W}$  and  $\lambda$ , i.e.,  $W^* = W^*(\tilde{W}, \lambda)$ , as are the optimal KKT multipliers  $\nu^* = \nu^*(\tilde{W}, \lambda)$  and  $\eta^* = \eta^*(\tilde{W}, \lambda)$ . Denote the set of nonzeros by  $\mathcal{A}$ .

**Non-Binding  $\ell_1$  Constraint** Suppose the  $\ell_1$  constraint is non-binding. Evaluating the subderivative on the left-hand side of the stationarity condition (8) gives

$$w_{jk}^* - \tilde{w}_{jk} = 0,$$

where we use that  $\nu^* = 0$  and  $\partial h(W^*) / \partial w_{jk}^* = 0$ . Differentiating this expression with respect to  $\tilde{w}_{qr}$  for  $(j, k) \in \mathcal{A}$ , gives

$$\frac{\partial w_{jk}^*}{\partial \tilde{w}_{qr}} = \delta_{jk}^{qr}.$$

For those  $(j, k) \notin \mathcal{A}$ ,  $w_{jk}^* = 0$  and hence

$$\frac{\partial w_{jk}^*}{\partial \tilde{w}_{qr}} = 0.$$

Moreover, because  $\nu^* = 0$ , we have

$$\frac{\partial w_{jk}^*}{\partial \lambda} = 0$$

for all  $(j, k)$ .



**Binding  $\ell_1$  Constraint - Active Set** Suppose the  $\ell_1$  constraint is binding and consider the gradients for  $w_{jk}^*$  in the active set. For these  $(j, k) \in \mathcal{A}$ , it follows from the stationarity condition (8) that

$$w_{jk}^* - \tilde{w}_{jk} + \nu^* \text{sign}(w_{jk}^*) = 0, \quad (10)$$

where we again use that  $\partial h(W^*)/\partial w_{jk}^* = 0$ . The complementary slackness condition (9) for  $(j, k) \in \mathcal{A}$  gives

$$\sum_{(j,k) \in \mathcal{A}} |w_{jk}^*| - \lambda = 0. \quad (11)$$

We proceed by first deriving the gradients of  $w_{jk}^*$  with respect to  $\tilde{w}_{qr}$ . Differentiating (10) with respect to  $\tilde{w}_{qr}$  gives

$$\frac{\partial w_{jk}^*}{\partial \tilde{w}_{qr}} - \delta_{jk}^{qr} + \frac{\partial \nu^*}{\partial \tilde{w}_{qr}} \text{sign}(w_{jk}^*) + \nu^* \frac{\partial}{\partial \tilde{w}_{qr}} \text{sign}(w_{jk}^*) = 0,$$

from which it follows

$$\frac{\partial w_{jk}^*}{\partial \tilde{w}_{qr}} = \delta_{jk}^{qr} - \frac{\partial \nu^*}{\partial \tilde{w}_{qr}} \text{sign}(w_{jk}^*). \quad (12)$$

Next, differentiating (11) with respect to  $\tilde{w}_{qr}$  gives

$$\sum_{(j,k) \in \mathcal{A}} \text{sign}(w_{jk}^*) \frac{\partial w_{jk}^*}{\partial \tilde{w}_{qr}} = 0. \quad (13)$$

Substituting (12) into (13) and solving for  $\partial \nu^*/\partial \tilde{w}_{qr}$  yields

$$\frac{\partial \nu^*}{\partial \tilde{w}_{qr}} = \frac{\text{sign}(w_{qr}^*)}{\sum_{(j,k) \in \mathcal{A}} \text{sign}(w_{jk}^*)^2} = \frac{1}{|\mathcal{A}|} \text{sign}(w_{qr}^*). \quad (14)$$

Finally, substituting (14) back into (12) gives

$$\frac{\partial w_{jk}^*}{\partial \tilde{w}_{qr}} = \delta_{jk}^{qr} - \frac{\text{sign}(w_{qr}^*) \text{sign}(w_{jk}^*)}{|\mathcal{A}|}.$$

We turn now to the gradients of  $w_{jk}^*$  with respect to  $\lambda$ . Differentiating (10) with respect to  $\lambda$  gives

$$\frac{\partial w_{jk}^*}{\partial \lambda} + \frac{\partial \nu^*}{\partial \lambda} \text{sign}(w_{jk}^*) + \nu^* \frac{\partial}{\partial \lambda} \text{sign}(w_{jk}^*) = 0,$$

from which it follows

$$\frac{\partial w_{jk}^*}{\partial \lambda} = -\frac{\partial \nu^*}{\partial \lambda} \text{sign}(w_{jk}^*). \quad (15)$$

Next, differentiating (11) with respect to  $\lambda$  gives

$$\sum_{(j,k) \in \mathcal{A}} \text{sign}(w_{jk}^*) \frac{\partial w_{jk}^*}{\partial \lambda} - 1 = 0. \quad (16)$$

Substituting (15) into (16) and solving for  $\partial \nu^*/\partial \lambda$  yields

$$\frac{\partial \nu^*}{\partial \lambda} = -\frac{1}{|\mathcal{A}|}. \quad (17)$$

Finally, substituting (17) back into (15) gives

$$\frac{\partial w_{jk}^*}{\partial \lambda} = \frac{\text{sign}(w_{jk}^*)}{|\mathcal{A}|}.$$

**Binding  $\ell_1$  Constraint - Inactive Set** Suppose the  $\ell_1$  constraint is binding and consider the gradients for  $w_{jk}^*$  in the inactive set. These  $(j, k) \notin \mathcal{A}$  play no role in either of the KKT conditions, and hence have no gradient with respect to  $\tilde{w}_{jk}$  or  $\lambda$ :

$$\frac{\partial w_{jk}^*}{\partial \tilde{w}_{qr}} = 0$$

and

$$\frac{\partial w_{jk}^*}{\partial \lambda} = 0.$$

□

## C PROOF OF PROPOSITION 1

*Proof.* The acyclicity constraints forces  $\|\omega_{jk}^h\|_2 = 0$  for some  $j$  and  $k$ , meaning the whole vector  $\omega_{jk}^h = 0$ . Likewise, the sparsity constraint, which represents a group lasso regularizer (Yuan and Lin 2006), is also known to set some  $\omega_{jk}^h$  to zero. Those surviving vectors that are not set to zero are shrunk towards zero by an amount  $\|\omega_{jk}^h\|_2 / \|\tilde{\omega}_{jk}^h\|_2$ . The combined effect of these two constraints gives that

$$\omega_{jk}^h = \tilde{\omega}_{jk}^h \frac{\|\omega_{jk}^h\|_2}{\|\tilde{\omega}_{jk}^h\|_2},$$

which equals zero if  $\|\omega_{jk}^h\|_2 = 0$ . Now, observe that the objective function can be expressed solely in terms of the norms of each vector:

$$\begin{aligned} \sum_{j,k} \|\tilde{\omega}_{jk}^h - \omega_{jk}^h\|_2^2 &= \sum_{j,k} \left\| \tilde{\omega}_{jk}^h - \tilde{\omega}_{jk}^h \frac{\|\omega_{jk}^h\|_2}{\|\tilde{\omega}_{jk}^h\|_2} \right\|_2^2 \\ &= \sum_{j,k} \left\| \tilde{\omega}_{jk}^h \left( 1 - \frac{\|\omega_{jk}^h\|_2}{\|\tilde{\omega}_{jk}^h\|_2} \right) \right\|_2^2 \\ &= \sum_{j,k} \|\tilde{\omega}_{jk}^h\|_2^2 \left( 1 - \frac{\|\omega_{jk}^h\|_2}{\|\tilde{\omega}_{jk}^h\|_2} \right)^2 \\ &= \sum_{j,k} (\|\tilde{\omega}_{jk}^h\|_2 - \|\omega_{jk}^h\|_2)^2. \end{aligned}$$

Taking  $\tilde{w}_{jk} = \|\tilde{\omega}_{jk}^h\|_2$  and  $w_{jk} = \|\omega_{jk}^h\|_2$  yields the claim of the proposition.

□

## D IMPLEMENTATION

ProDAG uses a multivariate Gaussian prior on  $\tilde{W}$  with independent elements, each having mean zero and variance one. The variational posterior on  $\tilde{W}$  is also taken as a multivariate Gaussian with independent elements, where the means and variances are initialized at their prior values. We use the Adam optimizer (Kingma and Ba 2015) with a learning rate of 0.1 to minimize the variational objective function. The posterior variances are held positive during optimization using a softplus transform. At each Adam iteration, 100 samples of  $\tilde{W}$  are drawn from the posterior to estimate the objective function. To project these sampled  $\tilde{W}$  and obtain  $W$ , we solve the projection using gradient descent with learning rates of  $1/p$  and  $0.25/p$  for the linear and nonlinear settings, respectively.

For the benchmark methods, we use open-source Python or Julia implementations:

- DAGMA: <https://github.com/kevinsbello/dagma>, Apache License 2.0;
- DiBS and DiBS+: <https://github.com/larslorch/dibs>, MIT License;
- BayesDAG: <https://github.com/microsoft/Project-BayesDAG>, MIT License; and

- PC: <https://github.com/mschauer/CausalInference.jl>, MIT License.

We use 50 particles for DiBS’s particle variational inference in the synthetic data examples and 10 particles in the real data example. More particles exceeded available memory.

The sparsity parameter  $\lambda$  of each method is tuned over a grid of 10 values between  $\lambda^{\min}$  and  $\lambda^{\max}$ .<sup>5</sup>

- ProDAG:  $\lambda^{\min} = 0$  and  $\lambda^{\max}$  is the average  $\ell_1$  ball from the learned posterior with  $\lambda = \infty$ ;
- DAGMA:  $\lambda^{\min} = 10^{-3}$  and  $\lambda^{\max} = 1$ ;
- DiBS and DiBS+: does not include a sparsity parameter;
- BayesDAG:  $\lambda^{\min} = 10$  and  $\lambda^{\max} = 10^3$ ; and
- PC: does not include a sparsity parameter.

The grids are chosen so that the learned sparsity level matches the true sparsity level for some value between  $\lambda^{\min}$  and  $\lambda^{\max}$ . For the real data example, we choose  $\lambda$  from the grid according to the sparsity level of the consensus graph. For the synthetic data examples, we choose  $\lambda$  using a separate validation set of size  $\lfloor 0.1n \rfloor$ . We could not extract the weighted adjacency matrices or neural networks from BayesDAG (only samples of binary adjacency matrices), so we choose its  $\lambda$  by revealing the true sparsity level.

In the nonlinear setting, the neural networks for ProDAG and DiBS consist of a single hidden layer with 10 neurons that use ReLU activation functions. DAGMA employs the same architecture but the neurons use sigmoid activation functions (its implementation does not support custom activation functions). The network for BayesDAG consists of two hidden layers, each with 128 neurons (its implementation does not support custom numbers of layers or neurons) that use ReLU activation functions.

The experiments are run on a Linux workstation with an AMD Ryzen Threadripper 3970x CPU, 256GB RAM, and two NVIDIA GeForce RTX 4090 GPUs. Individual experiments are run on either a single GPU or a single CPU core.

## E SIMULATION DESIGN

The synthetic datasets generated from linear DAGs are constructed as follows. We first randomly sample an Erdős–Rényi graph with  $p$  nodes and  $2p$  edges. The edges of this undirected graph are then oriented according to a randomly generated topological ordering. Each directed edge in the graph is then weighted by sampling weights uniformly on  $[-0.7, -0.3] \cup [0.3, 0.7]$ , yielding a weighted adjacency matrix  $W$ . We then draw the noise  $\varepsilon_1, \dots, \varepsilon_n$  iid as  $N(0, I)$  and finally generate the variables as

$$x_i = W^\top x_i + \varepsilon_i, \quad i = 1, \dots, n.$$

For synthetic datasets generated from nonlinear DAGs, we first sample an Erdős–Rényi graph and orientate it according to a random topological ordering. We then generate a feedforward neural network  $f_k$  with a single hidden layer of 10 neurons for  $k = 1, \dots, p$ . The weights of  $f_k$  are sampled uniformly from  $[-0.7, -0.3] \cup [0.3, 0.7]$ , with hidden layer weights of node  $k$ ’s non-parents set to zero. The activation is a ReLU. The noise  $\varepsilon_1, \dots, \varepsilon_n$  is drawn iid as  $N(0, I)$  and the variables are generated as

$$x_i = f(x_i) + \varepsilon_i, \quad i = 1, \dots, n,$$

where  $f(x) = (f_1(x), \dots, f_p(x))$ .

---

<sup>5</sup>The parameter  $\lambda$  in ProDAG refers to the  $\ell_1$  ball size, whereas  $\lambda$  in DAGMA and BayesDAG refers to the coefficient on the  $\ell_1$  penalty.